UNIVERSITÀ DEGLI STUDI DI PADOVA

Dipartimento di Fisica e Astronomia "Galileo Galilei"

Corso di Laurea in Fisica

Final dissertation

Supernova neutrino detection in JUNO, a large liquid scintillator neutrino detector

Thesis supervisor

Prof. Alberto Garfagnini

Thesis co-supervisor

Dr. Katharina Von Sturm

Candidate

Riccardo Triozzi

Academic Year 2020/2021

Contents

Abstract

The Jiangmen Underground Neutrino Observatory (JUNO) is a multi-purpose neutrino experiment under construction in South China. The 20 kton of highly transparent Liquid Scintillator (LS) are contained in an acrylic sphere surrounded by 17612 20" PhotoMultiplier Tubes (PMTs) and 25600 3" PMTs. JUNO aims at providing an energy resolution better than 3% at 1 MeV and thus offers exciting opportunities for addressing various important topics in neutrino and astroparticle physics. For instance, neutrinos play a crucial role during all stages of stellar collapse and explosion. The signature of a supernova explosion is a sudden increase of the neutrino interaction rate in the detector of several orders of magnitude (from below 1 kHz up to 1 MHz) for a short time O(1 s). Therefore the readout electronics has to withstand very high rates for a limited amount of time without data losses. The JUNO Padova research group is responsible for the design and development of the large PMTs readout electronics. The PMTs output signal is processed and stored temporarily in a local memory before being sent to the data acquisition, once validated by the trigger electronics. Besides the local memory situated in the readout-board FPGA, a 2 GBytes DDR3 SDRAM memory is available and it is used to provide a larger memory buffer in the exceptional case of a sudden increase of the input rate. A small experiment with 48 small size PMTs reading out the light coming from a 20 liter LS detector has been assembled at the *Legnaro National Laboratories* in Legnaro, Italy. Another setup has been built at the *Institute of High Energy Physics* in Beijing, China.
The first part of the thesis concerns the performance assessment of the electronics, carried out by simulating the production of high-rate scintillation photons in the LS and testing the highest rates sustainable by the system. By retrieving the amount of expected events and the number of correctly read events, it is possible to compute the efficiency of the setup at a fixed rate. This made it possible to understand the rate range in which the system can work and when the DDR3 is necessary.
Finally, rate measurements employing exclusively the DDR3 memory were collected thanks to a third setup at the *Department of Physics and Astronomy* in Padua, Italy. The purpose of this test is to understand whether the memory is capable of storing all the useful high-rate events by overrunning the usual data transfer bandwidth between the read-out electronics and the DAQ.

Chapter 1

Introduction

The Jiangmen Underground Neutrino Observatory (JUNO) is a large liquid scintillator neutrino detector currently under construction in southern China, that will detect electron antineutrino interactions produced by the nearby Nuclear Power Plants (NPP) thanks to the inverse beta decay reaction $\bar{\nu}_e + p \rightarrow e^+ + n$. The main goal of the experiment is the determination of the neutrino mass hierarchy to solve the Neutrino Mass Ordering (NMO) problem. Thanks to the excellent energy resolution (better than 3% at 1 MeV) and to the large fiducial volume it will be possible to address many important topics in neutrino physics such as the high precision measurements of neutrino oscillation parameters. With six years of data, the neutrino mass ordering can be determined at a $(3-4)\sigma$ significance and the neutrino oscillation parameters can be measured to a sub-percent precision [1].

1.1 Neutrino and Supernova Physics with JUNO

The relationship between the three flavour eigenstates neutrinos ν_e, ν_μ, ν_τ and the three mass eigenstates ν_1, ν_2, ν_3 can be written in terms of the 3×3 lepton mixing matrix U, usually referred to as the Pontecorvo-Maki-Nakagawa-Sakata (PMNS) matrix [2, 3]:

$$\begin{pmatrix} \nu_e \\ \nu_\mu \\ \nu_\tau \end{pmatrix} = \begin{pmatrix} U_{e1} & U_{e2} & U_{e3} \\ U_{\mu 1} & U_{\mu 2} & U_{\mu 3} \\ U_{\tau 1} & U_{\tau 2} & U_{\tau 3} \end{pmatrix} \cdot \begin{pmatrix} \nu_1 \\ \nu_2 \\ \nu_3 \end{pmatrix} \tag{1.1}$$

The PMNS matrix can be parametrized in terms of the three mixing angles θ_{13}, θ_{23}, θ_{12} and the CP-violating phase δ_{CP} and describes the neutrino-antineutrino oscillation in vacuum. Through the weak interaction neutrinos are created in a flavour eigenstate, which can be be determined as the coherent superpositions of the mass eigenstates. If neutrinos have non-zero masses, while travelling they can propagate independently and at a later time the combination of mass eigenstates does not correspond to the original flavour eigenstate. Neutrino oscillations are altogether described by θ_{13}, θ_{23}, θ_{12}, δ_{CP} and by two indipendent mass differences between the three mass eigenstates, Δm^2_{ij}. It is not clear whether the ν_3 neutrino mass eigenstate is heavier or lighter than the ν_1, ν_2 mass eigenstates: in the normal mass hierarchy the ν_3 is heavier, while in the inverted mass hierarchy the ν_3 is lighter. Employing the approximation $\Delta m^2_{32} \approx \Delta m^2_{31}$, the $\bar{\nu}_e$ survival probability can be written as

$$\begin{aligned} P_{ee} = 1 &- \cos^3\theta_{13} \sin^2 2\theta_{12} \sin^2 \Delta_{21} - \sin^2\theta_{13} \sin^2 |\Delta_{31}| \\ &- \sin^2\theta_{12} \sin^2 2\theta_{12} \sin^2 \Delta_{21} \cos 2|\Delta_{31}| \\ &\pm (\sin^2\theta_{12}/2) \sin 2\theta_{13} \sin^2 2\Delta_{21} \sin^2 2|\Delta_{31}| \end{aligned} \tag{1.2}$$

in which $\Delta_{ij} = \frac{\Delta m^2_{ij} L}{4E_\nu}$ [4]. The sign flip in the last term is due to the two neutrino mass hierarchy possibilites: the positive solution refers to the normal ordering, while the negative refers to the inverse

ordering. This effect is not negligible thanks to the large value for θ_{13} ($\sin^2(\theta_{13}) = (2.18 \pm 0.07) \cdot 10^{-2}$ [5]) and offers a method to discriminate the two possibilities.

Supernovae and neutrinos The detection of supernovae (SNe) neutrinos may play a crucial role in the determination of oscillation parameters and solving the mass hierarchy problem. Most of the supernovae are generally thought to explode through the same core-collapse mechanism and about 99% of the total explosion energy is released in the form of neutrinos. These are produced in or near the collapsing core of the star and traverse the outer layers of the star nearly unhindered [6]. The experimental signature of a SN explosion is a sudden increase in the neutrino interaction rate in the detector from below 1 kHz up to 1 MHz for a very short time of the order of 1 s. The two dozen neutrino events detected back in 1987 from Supernova 1987A [7] in Kamiokande-II, Irvine-Michigan-Brookhaven and Baksan experiments proved to be a unique source of information on the explosion mechanism of stars and helped affirm the current paradigm of neutrinos carrying out the energy and triggering the explosion. Given a reasonable rate of 1.63±0.46 galactic SNe per century, the probability for a detector to see one event is about 7.8%, 15.0%, 27.8% and 55.7%, assuming it stays constantly operational for 5,10,20 and 50 years respectively [8]. Therefore, when the next supernova occurs it will be crucial that the neutrino detectors will be capable to get the most of the signal through a good time resolution and a good reconstruction of the flux.

1.2 The JUNO Experiment

The JUNO experiment [1, 4] is located 43 km to the southwest of the Kaiping city, next to Jiangmen city in the Guangdong province, as shown in Figure 1.1.

Figure 1.1: Location of the JUNO experiment.

The site is situated equally far from the Yangjiang and the Taishan Nuclear Power Plant (NPP). The Day Bay NPP complex is 215 km away from the experiment and therefore it contributes about 6.4% of the reactors antineutrinos events in JUNO, considering oscillations. In absence of high mountains in the area where the sensitivty to the mass hierarchy is optimized, the detector will be deployed in an underground laboratory under the Dashi hill. Besides, a reference detector will operate at a few meters from the Thaishan reactor core to minimize systematic uncertainties bound to the reactor antineutrino beam. The Thaishan Antineutrino Observatory (TAO) [9] is a liquid scintillator detector designed to measure the reactor antinetruinos spectrum with high precision, having a critical role in the NMO determination.

1.2.1 The Experimental Apparatus

The JUNO detector is shown in Figure 1.2. The central detector (CD) consists of an acrylic vessel holding 20 kton of Liquid Scintillator (LS) and a PhotoMultiplier Tube (PMT) system. The central detector LS is contained in a spherical vessel of radius of 17.7 m. The total density of the LS is

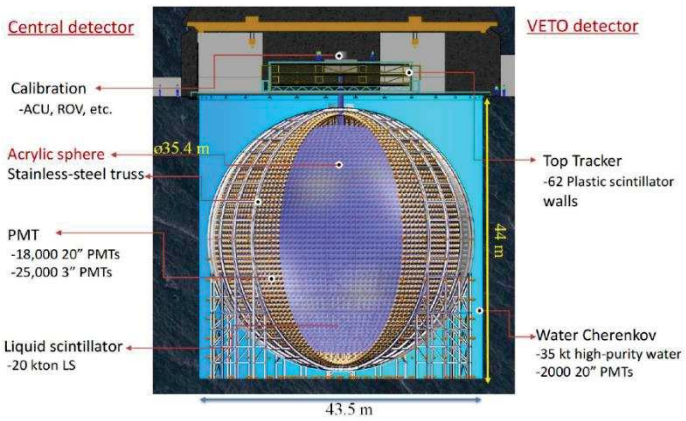

Figure 1.2: Schematic view of the JUNO detector.

0.859 g/mL: it mainly consists of Linear Alkyl-Benzene (LAB), a straight alkyl chain of 10-13 carbons attached to a benzene ring used for its great transparency, high flash points, good light yield and low chemical reactivity. On the other hand, the LS also contains 3 g/L 2,5-diphenyloxazole as the flour and 15 mg/L p-bis-(o-methylstyryl)-benzene as the wavelength shifter. In order to reach the expected energy resolution of 3% at 1 MeV, the LS attenuation length must be at least equal to 20 m at 430 nm. The scintillation light is picked up by 17612 large 20-inch PMTs and 25600 small 3-inch PMTs, installed on a spherical structure of radius of 19.5 m. The requirements for the PMTs photocatodes are a coverage greater than 75% and quantum efficiency at least equal to 35%.
The VETO detector will be divided into a top tracker (TT) and a water Cherenkov detector (WCD). Together the two detectors help reducing efficiently the background, primarily consisting of cosmic rays and environmental background particles. The WCD is a cylinder of 43.4 m in diameter and 44 m in height filled with 30 kton of ultrapure water that surrounds the CD. The expected muon tagging efficiency of the WCD is 99.5%. The TT is placed on top for the WCD and consists of scintillator strips grouped to form several modules, each with an expected efficiency of $(98.0 \pm 0.5)\%$.
Finally, the calibration system will provide different methods for calibrating the experiment and to have a checkup of the energy scale of the detector.

Readout electronics The JUNO electronics have to determine the time profiles and the energy of an event related to a photoelectron (PE) generated by a single large PMT: for a low-energy event one PE is produced and this ranges to thousands of PEs produced in high-energy events. An energy release of 1 MeV in the central detector corresponds to an average of about 1300 PEs and an energy resolution of 3% is expected. The readout electronics scheme is shown in Figure 1.3.

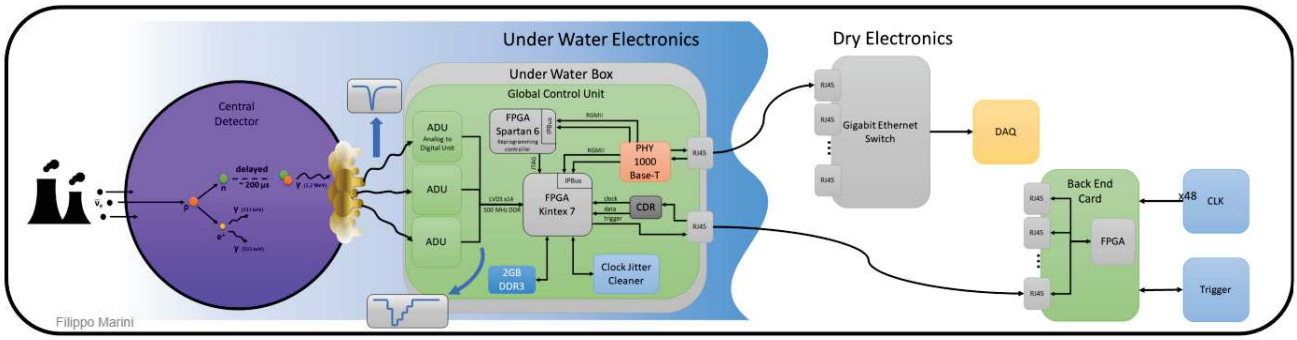

Figure 1.3: Scheme of JUNO readout electronics.

Groups of three PMTs are connected to underwater boxes containing three modules that generate the High Voltage (HV) from a low voltage input and the Global Control Unit (GCU), integrating Analogue to Digital Units (ADUs) and an FPGA. The GCU performs data digitization, buffering and

processing and also monitors and controls all the relevant parameters. The complete event information is distributed in the detector and each PMT can only collect it partially. The signals from the PMTs are received and analyzed online by the GCUs. Using a specific threshold level, it is determined whether there are any possible event fragment and a trigger request is sent through a synchronous link to the Back-End Card (BEC), specifically to the Trigger and Timing (TTIM) FPGA Mezzanine Card (FMC) that gathers the links coming from 48 GCUs. The TTIM is then connected to the Reorganize and Multiplex Unit (RMU), which interfaces with 20 BECs. Finally, the RMU connects to the Central Trigger Unit (CTU) that generates a trigger validation and sends it back to the GCUs: all the fragments of the events are transferred through Ethernet (asynchronous link) to the Data Acquisition (DAQ) system. In case of a supernova, the trigger rate will increase to a point where it is impossible to manage the data readout via Ethernet. Consequently, a buffer capable to store at least one second of raw data is implemented. To perform this task a DDR3 ram memory has been assembled in the GCU.

1.3 The JUNO Test Facilities

A small JUNO mock-up system has been built and is in operation to test the electronics at the *Legnaro National Laboratories* (LNL) of *National Institute for Nuclear Physics* in Legnaro, Italy. Additional measurements have been taken in another mock-up system set up at the *Institute of High Energy Physics* (IHEP) of the *Chinese Academy of Science* in Beijing, China. Both setups have been employed to characterize the electronics.

The JUNO test facility at LNL The LNL facility is shown in Figure 1.4. The internal cylindrical vessel is made of transparent Plexiglas, containing roughly 17 L of LS, composed by a mixture of a LAB solvent with Poly-Phenylene Oxide and p-bis(o-MethylStyryl)-Benzene, used as wavelength shifter. The cilinder is surrounded by 48 PMTs with a diameter of roughly 5 cm, connected in groups of 3 to 16 GCUs, each with three channels. There are 3 Plastic Scintillators (PSs), one on top of the apparatus and the others on the bottom of the plastic structure that supports the PMTs. The PSs are used as a trigger mechanism based on cosmic rays employing the coincidence of these scintillators. Finally, a LED source is located on top of the detector using an optical fiber, providing light at 405 nm.

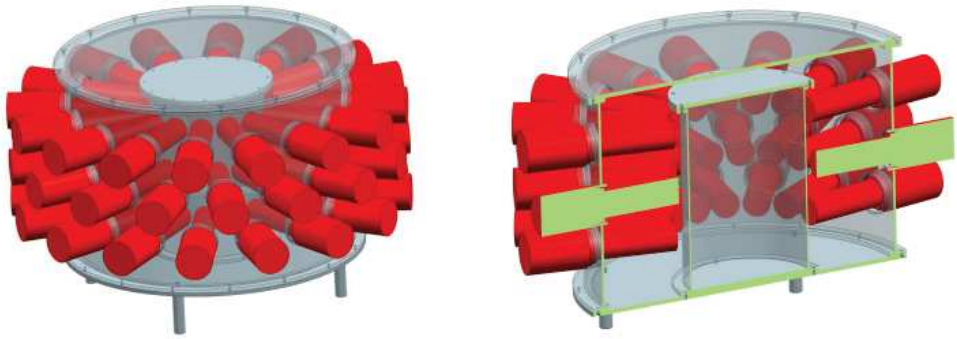

Figure 1.4: Design of the JUNO test facility setup at the Laboratori Nazionali di Legnaro.

The electronics chain scheme is shown in Figure 1.5. For the measurements considered in this thesis work 11 GCUs were employed, resulting in 33 fully working acquisition channels that collect signals asynchronously. Thanks to the Analog-to-Digital Unit (ADU), the analog signal produced for each channel is digitized and then doubled: one signal copy is registered with the corresponding GCU timestamp into a L1 cache, the other copy is analyzed using a trigger algorithm. If the signal is consistent with the chosen threshold, a trigger request is sent to the BEC which can validate the trigger decision, sending back the same timestamp to all involved GCUs. In the first part of this work, the presented measurements are obtained using the *External Trigger Mode*. Therefore, the trigger

request is considered valid when it coincides with the external trigger generated by the HP Agilent Keysight 8116A pulser within a predefined time window and it is sent directly to the BEC. Finally, the signals with the selected timestamp is transferred from the cache to the First-In-First-Out (FIFO) unit and then moved to the PC through an Ethernet switch, where the DAQ stores the raw data.

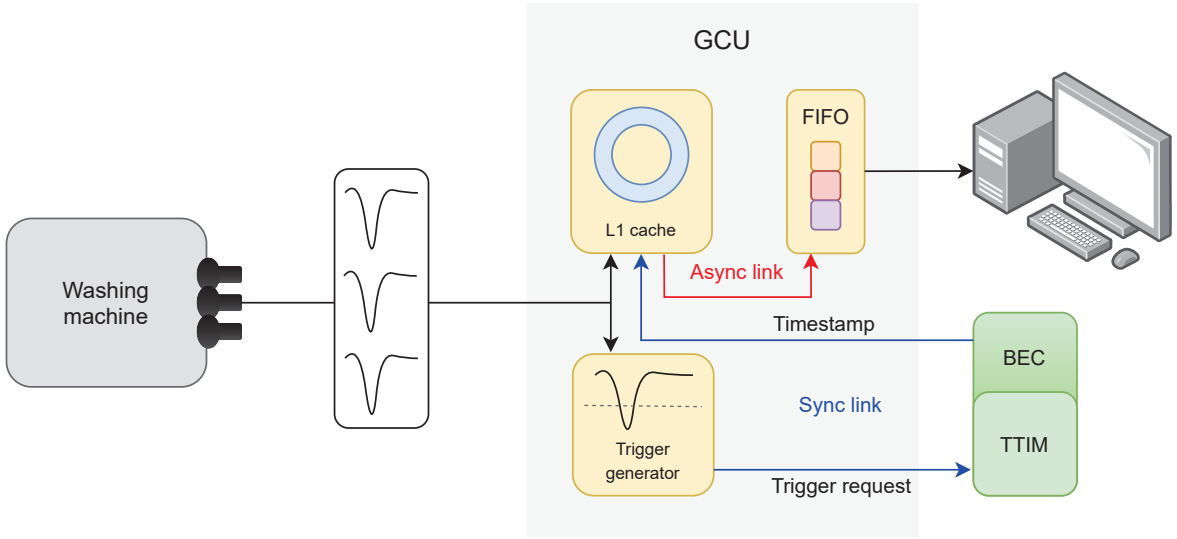

Figure 1.5: Scheme of the Legnaro electronics chain; *washing machine* is a nickname for the experimental apparatus with the LS and 48 PMTs.

The JUNO test facility at IHEP Another mock-up system has been set up at IHEP in Beijing, using 10 GCUs and without employing the LS or PMTs. Similarly to the LNL system, other than the GCUs the full electronics chain is composed of one BEC, RMU and CTU.

Chapter 2

Efficiency Tests

In the course of this thesis work various measurements have been taken with different trigger rates. During an high rate acquisition it is clear that the system is not capable of storing all of the produced events correctly and this results in missing information for some of the active channels. Therefore, in this chapter many tests are carried out by calculating the *efficiency* or *survival fraction*, given by the amount of events effectively received over the total number of events expected.

2.1 Data Acquisition: preliminary results

The data acquired from each channel of the GCUs are stored in binary files and are organized in *data packets*, each one having a variable number of *words*, defined as sequences of 16 bits. Any packet is wrapped by an *header* and a *trailer*, which are formed by 8 words. These two sequences allow to separate different data packets and provide unique information on each packet. The structure of header and trailer is reported below.

Header	
0x805a	← Fixed header start
0x0002	← Channel number (0,1,2)
0x0040	← Trigger window
0x85c9	← Trigger count
0x0000	
0x0018	← Timestamp
0x2dd4	
0xee03	

Trailer	
0x55aa	
0x0123	
0x4567	← Fixed trailer starting sequence
0x89ab	
0xcdef	
0xff00	
0x0002	← GCU ID
0x0869	← Fixed trailer end

Each header starts with a fixed hexadecimal number; the GCU channel number (0, 1 or 2), the trigger window and the trigger count are then reported. The trigger window is also referred to as the packet size and indicates the data packets' size including header and trailer in units of 8 words. The trigger count is cyclic: hexadecimal representation ranges from 0 to 65535 and when the maximum value is reached, the trigger number starts over from 0. Finally, the last 64 bit sequence is the timestamp, which gives the time reference in units of 8 ns. The trailer is composed by a fixed starting sequences consisting of 6 words, the GCU ID number and the fixed trailer ending word. The actual data is stored as a sequence of words given by the trigger window minus header and trailer and depicts the signal waveform, which starts from the reference timestamp found in the header. Each word corresponds to one nanosecond: to express the waveform size in nanoseconds we subtract the trigger window by 2 (header and trailer size in unit of 8 words) and then we multiply it by 8.

2.1.1 Raw Data Analysis

The binary files are read using a ROOT [10] based program, which identifies the data packets and stores the acquired information in ROOT `TTree` objects; the survival fraction is then computed. Firstly, a *single channel analysis* is performed on the raw data. The number of events actually read is calculated by means of the trigger count number provided in the header sequence. While in low rate acquisitions the trigger number progressively increases by one unit, using high rates the system is not able to read effectively all the events and this results in various trigger numbers skipped. The expected amount of events is then computed using the last stored event's trigger count. Such an analysis provides a survival fraction value for each channel: since we expect that any channel approximately loses the same amount of events, the arithmetic mean of those values is considered. Nevertheless, the just described process does not account for correlation between different channels of the GCUs. Besides, the *event building analysis* is carried out by keeping track of when the system fails in providing a specific timestamp from all active channels. The number of effectively read events is computed by considering only the case in which all channels of the GCUs have not lost a timestamp. In this way, we expect that the efficiency at high acquisition rates in case of event building analysis is consistently lower compared to the single channel analysis case. On the other hand, at very low rates the survival fraction trends as function of the rate are equal in the two scenarios and the two begin to differ when the efficiency drops from 1. A comparison of the scenarios is represented in Figure 2.1, in which the analyzed data refers to the acquisition with one GCU and three active channels. The trigger window is set to 120, which corresponds to a waveform with a duration of 944 ns. Here, the efficiency drops consistently from around 7 kHz. Moreover, the top x-axis indicates the *bandwidth*, computed by multiplying the rate by the number of acquisition channels and by the trigger window expressed in bits. The former term is obtained by multiplying the header's trigger window by 8 (since it is expressed in units of 8 words) and by 16 (each words consists of 2 bytes, i.e. 16 bits). In this case, the drop in efficiency takes place at around 302 Mb/s.

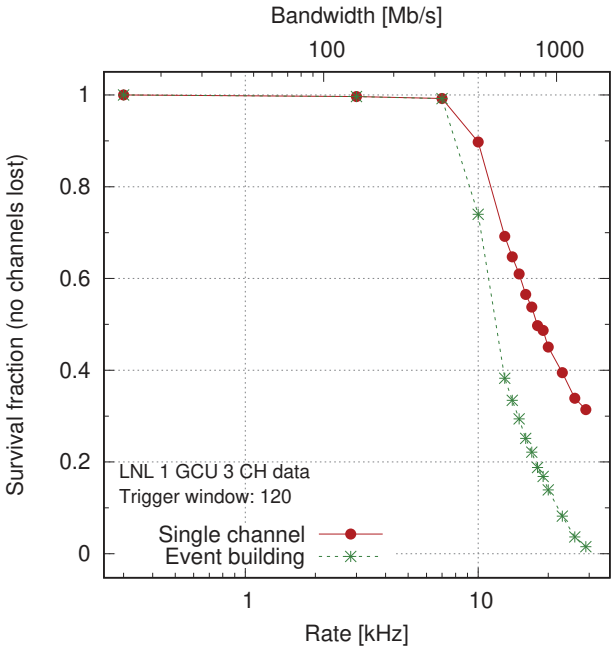

Figure 2.1: Survival fraction as function of the acquisition rate and bandwidth (1 GCU, 3 channels data). Data readout with 1 process per GCU and buffer length set to 2048 (for reference, see Section 2.1.2).

2.1.2 Data Readout

During data acquisition and readout it is possible to vary some parameters in the provided DAQ softwares; by doing so we found that the survival fraction trend as a function of rate is sensibly altered. Firstly, two different version of the DAQ software were available. In the first version, the system employed one process for each channel resulting in three processes for the whole GCU: in the course of this work this case will be denoted as *CH readout*. In the most recent version, denoted as *GCU readout*, the software used a single process for the whole GCU. Furthermore, it is possible to change the length parameter of the *memory buffer*, in which the first chunk of data read by the DAQ software is temporarly stored. To test the efficiency, data between 500 Hz and 30 kHz was acquired with different combinations of setup settings. A comparison of the survival fraction trends as a function of the external trigger rate and bandwidth varying type of readout and buffer size is rendered in Figure 2.2, which refers to data from 11 GCUs with 33 acquisition channels analyzed by looking at individual channels. The trigger window is set to 40, that is a waveform of 304 ns. Firstly,

it is noticeable that the efficiency trends in the two CH and GCU readout scenarios are highly similar. In both cases, the drop from 100% is at around 10 kHz or 1690 Mb/s. Along the descent, the GCU readout seems slightly less efficient. Since the trends are close, the two types of readout are both employed during this work. On the other hand, using the GCU readout the buffer length, expressed in units of 32-bit blocks, was changed to 512 and 2048 . It is evident that the survival fraction is heavily reduced in case of a smaller buffer size: in this case the drop takes place at around 5 kHz or 840 Mb/s. This is due to the fact that reading the events has a computational cost and by employing a smaller buffer size more cycles are needed. Therefore, from now onward the buffer length is set to its maximum value, namely 2048.

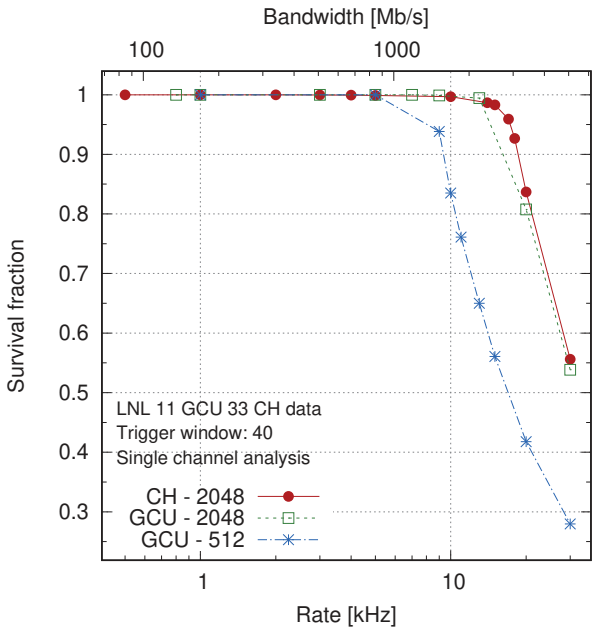

Figure 2.2: Survival fraction as function of the acquisition rate and bandwidth (11 GCUs, 33 channels data).

2.1.3 ControlHub Discussion

It is worth noticing that our system employed the IPbus protocol developed at CERN for data transmission through Ethernet [11]. Throughput, defined as the amount of data transferred per unit of time, is an important parameter that characterizes the control system and is around 400 Mb/s for payload sizes of the order of 100 kB. In particular, ControlHub is a software application within the IPbus suite that mediates simultaneous hardware access from multiple control applications to one or more devices. It implements the IPbus reliability mechanism for the ControlHub-device User Datagram Protocol (UDP) packets: any loss re-ordering or duplication of the IPbus UDP packets is automatically corrected by the ControlHub [11]. In our case, there are two different servers available for acquisition. Acquiring data through the old server allows to disentangle ControlHub from acquisition: a comparison be-

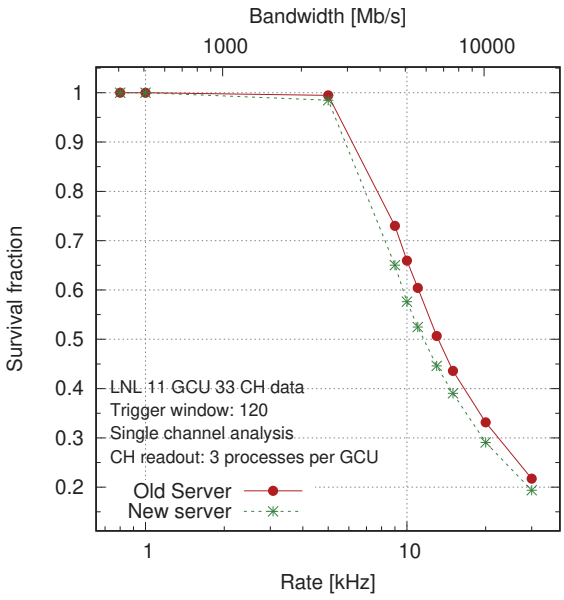

Figure 2.3: Survival fraction as function of the acquisition rate and bandwidth (11 GCUs, 33 channels data).

tween data taking through old and new server is shown in Figure 2.3, with data acquired from 11 GCUs and 33 channels. The trigger window is set to 120, corresponding to a waveform of 944 ns. In both cases the efficiency starts to decrease at about 5 kHz or 2530 Mb/s. At higher frequencies, the survival fraction linked to the new server is systematically lower: this could be linked to the fact that in the new server ControlHub is not disentangled from acquisition and this adds more processes and thus stress on the CPU, resulting in slightly more events lost. Even if the two efficiency trends are akin, the measurements presented in the following sections are collected through the old server.

2.2 Efficiency of the JUNO Test Facilities

In the previous section an outline of data acquisition modes and fundamental parameters has been provided. At this point various rate measurements were collected to characterize the electronics chain response: resulting data were analyzed using event building analysis.

2.2.1 Rate Measurements and Waveform Size

First of all, rate data were collected setting the trigger window to 40, 80 and 120, corresponding respectively to the waveform sizes of 304 ns, 624 ns and 944 ns. The efficiency values calculated and plotted in Figure 2.4 are related to data from 1 GCU and 3 channels readout with one process per GCU. By varying the trigger window, it is possible to change the size of the waveform and by doing so the survival fraction trend as a function of rate is consistently shifted. As a matter of fact, at a fixed frequency a higher waveform size corresponds to a lower survival fraction: this is evident in Figure 2.4a. At low rates the efficiency trends are alike and the system begins to skip events at approximately 7 kHz, 12 kHz and 20 kHz. On the other hand, it is clear that data scale if we calibrate the x axis to show the bandwidth as depicted in Figure 2.4b: the three survival fraction trends as a function of the bandwidth are overlapped. This has to do with the fact that the GCUs output the same amount of information per unit of time independently of the chosen waveform size. In this case, the efficiency drop from 1 at around 360 Mb/s.

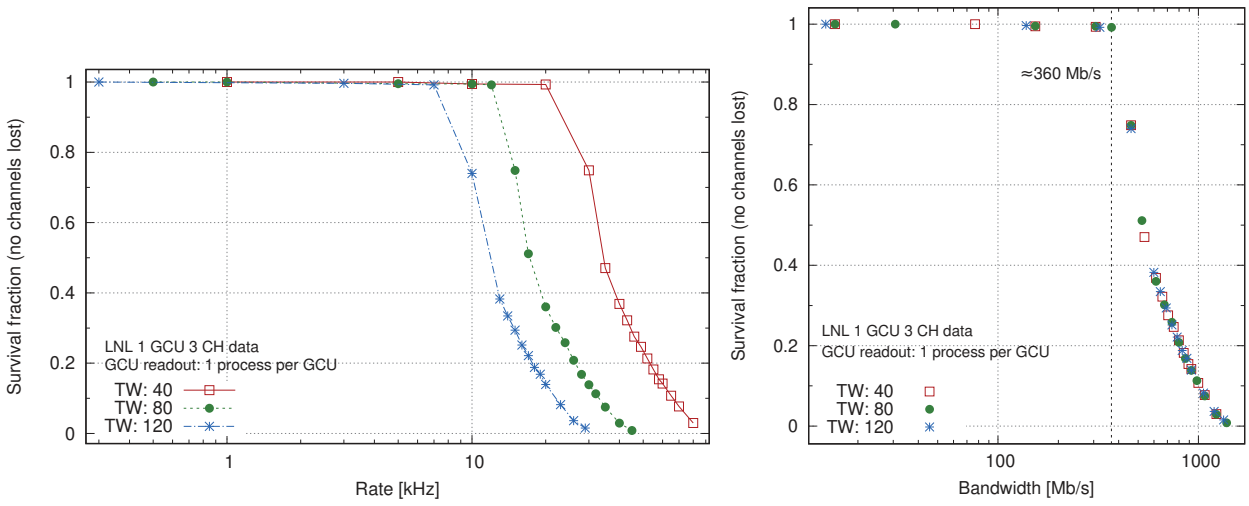

(a) Trend as function of trigger rate.

(b) Trend as function of bandwidth.

Figure 2.4: Survival fraction as function of the acquisition rate and bandwidth (1 GCU, 3 channels data).

2.2.2 Rate Measurements at IHEP

In this section results regarding rate measurements with 1 GCU and 3 acquisition channels are presented. The trigger window is fixed to 40, resulting in a waveform size of 304 ns; data were readout with three processes per GCU. Plots of the survival fraction trends as function of trigger rate and bandwidth are shown in Figure 2.5. In particular, Figure 2.5a depicts the survival fraction computed using both LNL and IHEP data. The trend as function of rate is almost identical in the two scenarios.

The result is in line with the expectations, since the two test facilities were set up to achieve equal results. Furthermore, the drop in efficiency takes place at approximately 30 kHz or 460 Mb/s: the theoretical limit of $400 - 500$ Mb/s throughput for a 304 ns waveform is thus reached [11].

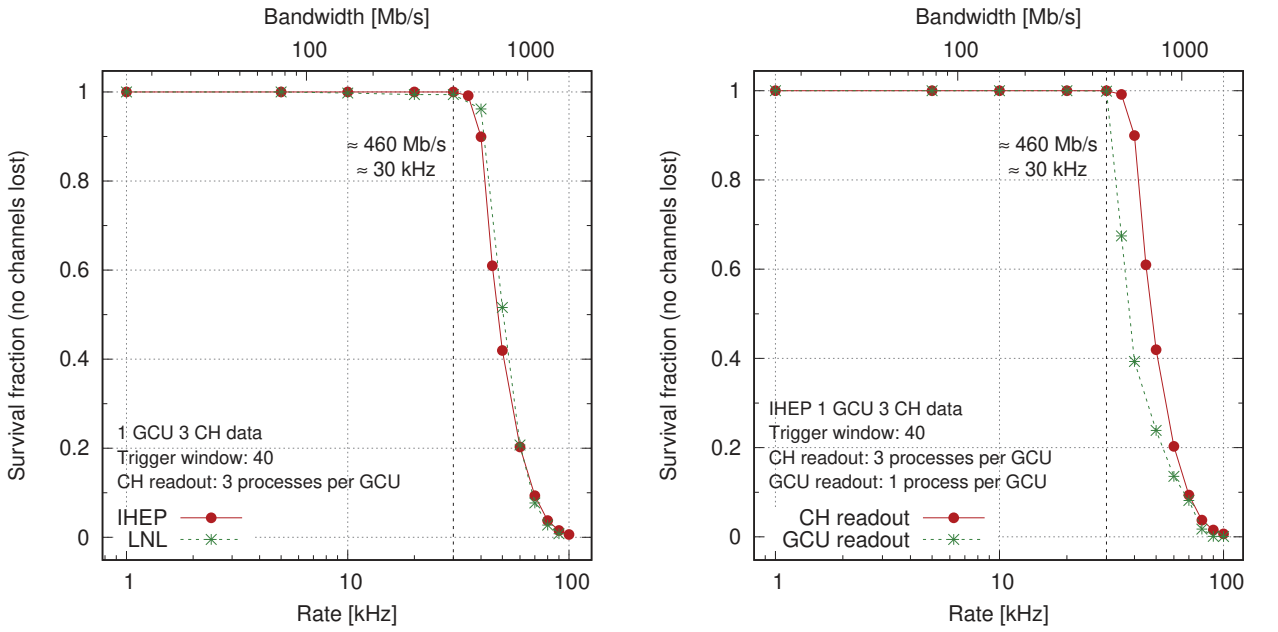

(a) Comparison between LNL and IHEP measurements.

(b) Comparison between CH and GCU readout (IHEP measurements).

Figure 2.5: Survival fraction as function of the acquisition rate and bandwidth (1 GCU, 3 channels data).

On the other hand, Figure 2.5b represents the efficiency trend comparing CH and GCU readout. The survival fraction trends with respect to the two readouts, while remaining somewhat similar, seems slightly more shifted if compared to the similar comparison for LNL data (Figure 2.2). However, the trends at low rates are still alike and the system starts losing information at around 30 kHz or 460 Mb/s in both cases. After the fall, the trends come back akin in the high frequency tail.

2.2.3 Rate Measurements with Several GCUs

Finally, rate measurements employing several GCUs are rendered in Figure 2.6.

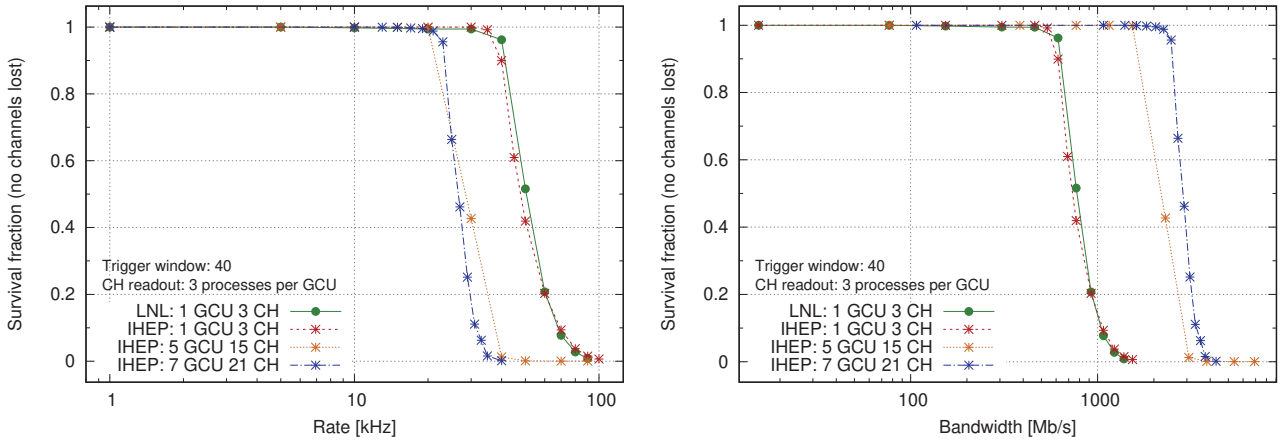

(a) Trend as function of trigger rate.

(b) Trend as function of bandwidth.

Figure 2.6: Survival fraction as function of the acquisition rate and bandwidth (11 GCUs, 33 channels data).

In particular, we collected data using 1 GCU (3 channels), 5 GCUs (15 channels) and 7 GCUs (21

channels) at the IHEP facility; data taken at LNL with 1 GCU and 3 channels are also presented for reference. In all cases the waveform size is fixed to 304 ns. As pictured in Figure 2.6a, by increasing the number of GCUs and thus acquisition channels the survival fraction at a fixed rate is lower. Consequently, if we employ a large number of GCUs for data taking the frequency range in which no information is lost (i.e. survival fraction is equal to 1) is much more limited. As a matter of fact while the efficiency drop for the 1 GCU measurements takes place at around 30 kHz as previously discussed, the drop for 5 and 7 GCUs is around 20 kHz. Contrastingly, as shown in Figure 2.6b the total bandwidth increases by using a larger amount of GCUs and specifically the efficiency trend as function of bandwidth scales by a factor equal to the number of GCUs. In this case the drop takes place at around 460 Mb/s, 1540 Mb/s and 2150 Mb/s respectively.

Chapter 3

DDR3 SDRAM Efficiency Test

As previously mentioned, a dedicated 2 GByte Double Data Rate 3 (DDR3) Synchronous Dynamic Random Access Memory (SDRAM) module has been implemented into the GCU.

3.1 Electronics Chain

The rate measurements presented in this chapter were taken in a third test facility set up at the *Department of Physics and Astronomy* of the *Univeristy of Padua* in Padua (PD), Italy. The electronics chain is schematized in Figure 3.1.

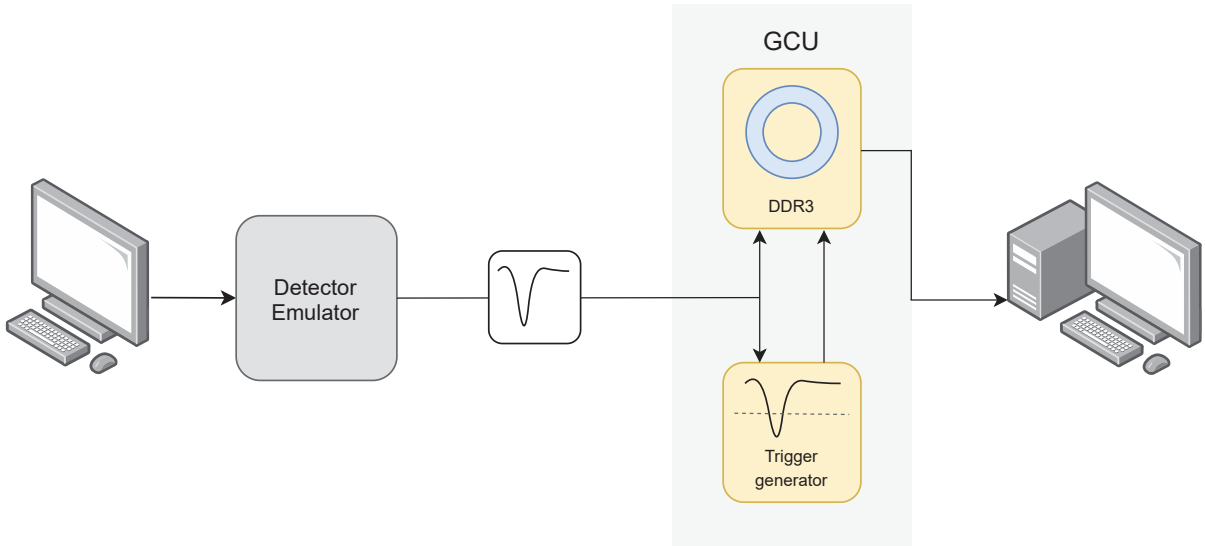

Figure 3.1: Scheme of the Padua electronics chain.

The impulses analyzed by the trigger generator system are produced by the CAEN DT5810D Dual Fast Digital Detector Emulator [12]. Through a dedicated user interface it is possible to fine-tune the pulse parameters. The negative impulse is 1 V low and is characterized by a rise time of 10 ns and a decay time of 5 ns; the rate parameter is manually changed before each measurement. The emulator's output is then redirected into the GCU. At this point, the FIFO is not readout and rapidly fills up: a customized *High Event-Rate Path* in the GCU is thus followed. Firstly, the DDR3 packager module encapsulates the events with a header and a trailer. The data is then sent to the controller, that fills the DDR3 like a circular buffer: if the memory fills up while the system is still writing, the content will be overwritten. When the DDR3 is readout, writing is stopped and will resume once the whole memory is emptied out by the DAQ module. It is worth noticing that the DDR3 is filled in

Auto Trigger Mode, hence there is no need for the L1 cache. More explicitly, any event that exceeds a specific threshold is transmitted to the BEC, but there is no need for any trigger validation message from it.

3.2 DDR3 Rate Measurements

In the previous chapter, it was found that the system is able to collect data without losing any event at low rates, specifically up to the order of a few kHz based on how many GCUs are employed and thus how many acquisition channels are readout. This information is crucial, for instance, in calibration acquisitions with radioactive sources with rates of the order of kHz. The characterization of the electronics chain also helps understanding the rate range in which the system can effectively work without losing information and thus when it is necessary to employ the DDR3 memory. Therefore, measurements were collected by setting the rate to values from the order of tens of kHz up to 15 MHz, with one acquisition channel. Since the pulse is about tens of nanoseconds wide, the highest testable rate is around $10 - 100$ MHz so that consecutive impulses do not overlap. It is possible to estimate the time it takes to fill up the memory by dividing its size by the trigger window (all expressed in bytes or bits) and by the rate. Once the memory is filled with events of interest at a fixed frequency, it can be readout. The pre-trigger parameter is fixed to 30 and the trigger window is set to 50 for the whole data taking process. The corresponding waveform size is equal to 384 ns.

3.2.1 Data Structure and Analysis

The raw data structure of the DDR3 readout generally differs from the usual acquisition data format (see Section 2.1 for reference), while some features remain the same. The binary files are still organized in data packets with a variable number of words, i.e. sequences of 16 bits. Moreover, the header and trailer sequences are identical in the two acquisition modes. On the contrary, in the DDR3 raw data all channels are included in a single file; the channel number can be retrieved in the header. Finally, the order in which the data is stored in the binary file is inverted in groups of 8 words, or 128 bits, while the order within any 128 bits block is preserved. Given a number n of acquired events, the overall data structure is reported on the side: in the DDR3 case the first read event is actually the last event that was written on the memory and the payload is reversed accordingly. To perform the raw data analysis, in the first place the data linked to different channels have to be split in different binary files. Each file is then appropriately reversed with a dedicated program and the same ROOT based software mentioned in Section 2.1.1 is exploited to store acquired information in ROOT `TTree` objects.

Normal
Header 1
Payload 1
Trailer 1
...
Header n
Payload n
Trailer n

DDR3
Trailer n
Rev. Payload n
Header n
...
Trailer 1
Rev. Payload 1
Header 1

3.2.2 Efficiency Test

In order to characterize the efficiency of the system writing on the DDR3, the survival fraction is computed. It should be mentioned that unlike the normal acquisition discussed in the previous chapter, even in case of lost events the DDR3 is programmed not to skip the trigger number, which remains consecutive. It is thus necessary to carry out the analysis by keeping track of the timestamps provided in the header sequence. An appropriate range of acquired events is sorted and the timestamps linked to first and last event are retrieved from the `TTree` object. The time interval related to the acquisition is determined by the last event's timestamp minus the first one and has to be opportunely converted into seconds, knowing that the timestamps are expressed in units of 8 ns. It is then possible to determine the efficiency as the amount of events effectively fetched (equal to the chosen range) over the number of expected events. To obtain the latter term, we multiply the acquisition time interval by the selected rate. The efficiency trend as function of the acquisition rate and bandwidth is shown in Figure 3.2.

At rates of the order of tens of kHz up to around 1.5 MHz the system is able to collect data without losing any useful information. Therefore the *High Event-Rate Path* in the GCU is successful in replacing the normal acquisition mode, which on the other hand led to missing information in the stored data at rates of the order of a few KHz as discussed in the previous chapter. It should be recalled that in case of a supernova explosion, the neutrino interaction rate in the detector increases up to about 1 MHz for a few seconds. The DDR3 seems to manage frequencies of this magnitude with an efficiency of 100% and is also able to store about 1 second worth of data, hence the system behaves as expected. Finally, the survival fraction drop takes place at around 1.5 MHz or 9.2 Gb/s.

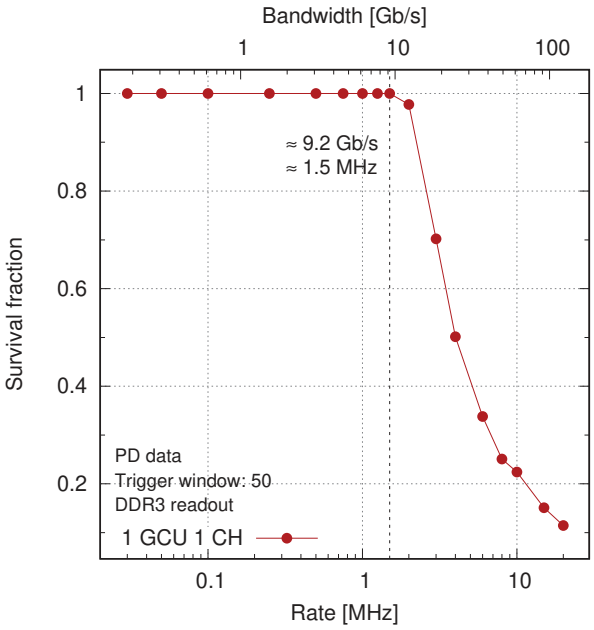

Figure 3.2: Survival fraction as function of the acquisition rate and bandwidth (1 GCU, 1 channel data). The signal window is 384 ns wide.

3.3 Remarks on the DDR3 readout

3.3.1 Data Quality Check

In order to perform a data quality check and verify that the data acquisition was carried out as expected, it is possible to graphically inspect the trigger number and timestamp of the acquired events. An example of the trends as function of the event number is pictured in Figure 3.3, for which only a fragment of the DDR3 data with a rate equal to 30 kHz was considered.

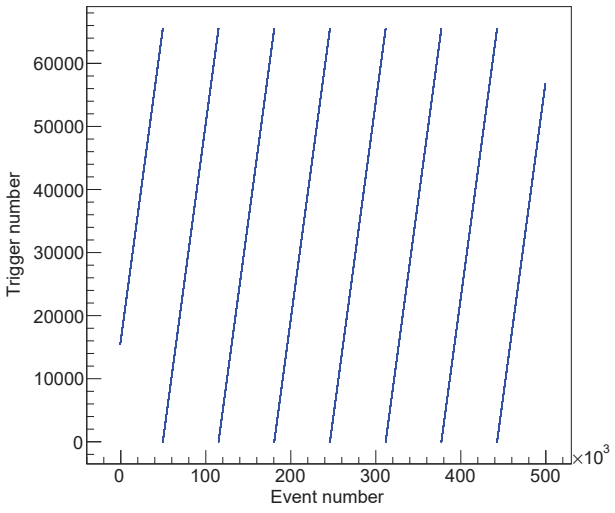

(a) Trigger number trend as function of event number.

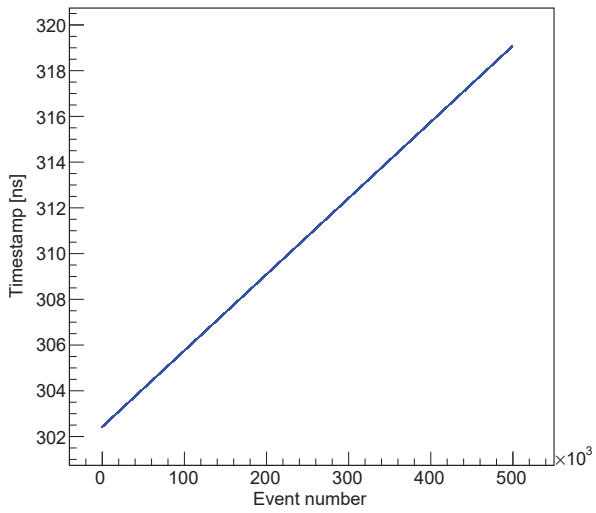

(b) Timestamp trend as function of event number.

Figure 3.3: Example of data quality check plots. Data from DDR3 acquisition with 30 kHz rate.

In Figure 3.3a the trigger number increases linearly and once the count reaches 65535, namely the

maximum number in hexadecimal representation, it starts over from 0. This occurrence was already introduced in Section 2.1. It is worth recalling that the trigger count increases by a unit with consecutive events, since the DDR3 is programmed not to skip any number even in case of data losses. On the other hand, Figure 3.3b shows the timestamp trend, in which the values are properly converted into nanoseconds. The data depicted in this plot are used to carry out the efficiency analysis presented in Section 3.2.2. Moreover, these data can be used to inspect the rate and check whether it coincides with the one set during acquisition. To achieve this, the time interval between two consecutive events is computed, subtracting the event's timestamp by the preceding one. The reciprocal of the time intervals should roughly correspond to the chosen frequency.

3.3.2 Acquisition Modes Comparison

Finally, the Padua setup was used to perform a normal acquisition with the purpose of comparing the resulting acquired waveform with the one obtained through the DDR3 acquisition. It was made use of the Detector Emulator, setting up an impulse with the same characteristics as described in Section 3.1. The rate was set to a low value as 10 Hz: in the normal acquisition the FIFO memory is much smaller than the DDR3 and rapidly fills up. The acquisition is once again carried out in *Auto Trigger Mode*. The pre-trigger and trigger window parameters were set to 30 and 40 respectively. The waveform plots from single data packets linked to the two acquisition modes are shown in Figure 3.4 and can be qualitatively compared.

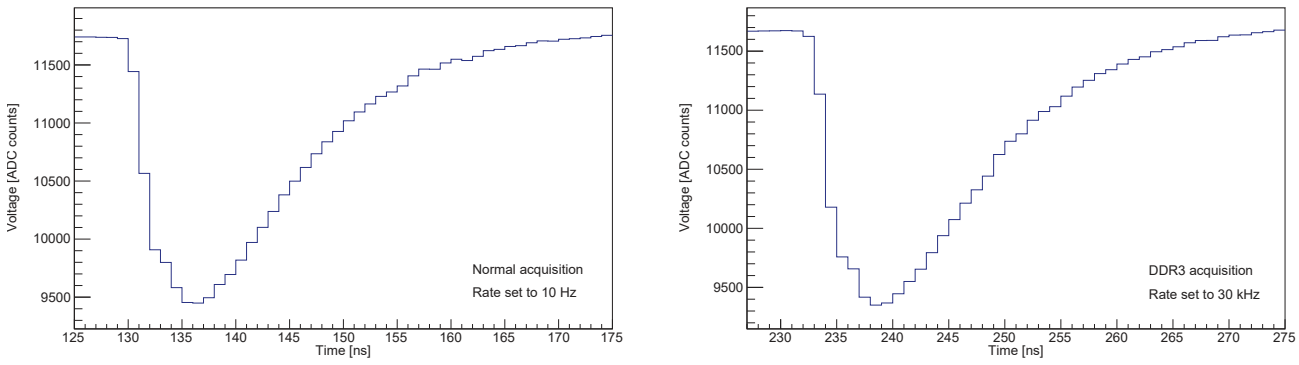

(a) Normal acquisition with a rate of 10 Hz.

(b) DDR3 acquisition with a rate of 30 kHz.

Figure 3.4: Example of waveform plots obtained with different acquisition modes.

The y-axis indicates the voltage, provided in units of Analog To Digital Converter (ADC) counts, and it can be noted that the signal baselines roughly have the same value in both acquisition modes. Moreover, the signal are approximately 40 ns wide in the two cases. The displacement along the x-axis is linked to the different pre-trigger and trigger window values and does not impact the overall signal trend.

Conclusions

In the course of this thesis, several rate measurements were collected with the purpose of studying the electronics' response to high frequencies. To achieve this, three setups in Legnaro, Padua and Beijing were exploited.
In the first part, data were taken at LNL and IHEP by varying the external trigger rates. The two facilities were set up to achieve equal results and this was tested as well. By computing the survival fraction of the correctly acquired events over the total amount expected, it became evident that the setups were not able to fetch all the useful information at rates of the order of the kHz. The highest bandwidth and frequency the system could withstand were characterized by numerous parameters. For instance, changing the memory buffer size prior to the readout severely impacted the efficiency trend as function of rate and bandwidth. Moreover, the survival fraction trend as function of acquisition rate shifted noticeably by varying the trigger window (size of the data packets). Once calibrated the x-axis to show the bandwidth, the different trends lined up. It was also possible to carry out the readout with two different software, characterized by different amount of processes employed: this sensibly altered the survival fraction at a fixed rate or bandwidth. It is noteworthy that the setups exploited the IPbus protocol and specifically its ControlHub application: by disentangling its execution from acquisition the efficiency slightly improved. Finally, rate measurements with 1, 5 and 7 Global Control Units were collected with all the available acquisition channel. By increasing the number of GCUs the efficiency at a fixed frequency is much lower, limiting the rate range in which the setups work as expected. On the other hand, at a fixed bandwidth the survival fraction is much higher and scales with a factor equal to the number of GCUs used. The highest rate and bandwidth the test facilities could withstand with 1 GCU and 3 active channels were respectively around 30 kHz and 460 Mb/s.
In the last part of the thesis, additional measurements were taken expoliting the DDR3 SDRAM memory at a third setup at the University of Padua. By following a dedicated *High Event-Rate Path* in the GCU it was possible to correctly store events up to about 1.5 MHz or 9.2 Gb/s, hence the system is capable of sustaining neutrino bursts in case of a supernova without losing too much useful information.
Regarding future perspectives, it is planned to implement the *jumbo frame* feature in the IPbus suite, namely Ethernet frames with up to 9000 bytes of payload (overrunning the IEEE 802.3 standard of 1500 bytes per payload) [13] to improve the efficiency of the test facilities' electronics. Finally, the DDR3 will be tested with more than one channel and GCU.

Bibliography

[1] A. Abusleme et al. *JUNO Physics and Detector*. Accepted by Progress in Particle and Nuclear Physics. 2021. arXiv: 2104.02565 [hep-ex].

[2] Z. Maki, M. Nakagawa, and S. Sakata. "Remarks on the unified model of elementary particles". In: *Progress of Theoretical Physics* 28 (1962), pp. 870–880. DOI: 10.1143/PTP.28.870.

[3] B. Pontecorvo. "Neutrino Experiments and the Problem of Conservation of Leptonic Charge". In: *Zh. Eksp. Teor. Fiz.* 53 (1967), pp. 1717–1725.

[4] F. An et al. "Neutrino physics with JUNO". In: *J. Phys.* 43.3 (Feb. 2016), p. 030401. ISSN: 1361-6471. DOI: 10.1088/0954-3899/43/3/030401. arXiv: 1507.05613.

[5] P. A. Zyla et al (Particle Data Group). In: *Progress in Particle and Nuclear Physics* (2020), p. 083C01.

[6] Jost Migenda. "Supernova Model Discrimination with Hyper-Kamiokande". 2020. arXiv: 2002.01649 [astro-ph.IM].

[7] A. Suzuki. "The 20th anniversary of SN1987A". In: *J. Phys. Conf. Ser.* 120 (2008), p. 072001. DOI: 10.1088/1742-6596/120/7/072001.

[8] A. Gallo Rosso. "Supernova neutrino fluxes in HALO-1kT, Super-Kamiokande, and JUNO". In: *Journal of Cosmology and Astroparticle Physics* 2021.06 (June 2021), p. 046. ISSN: 1475-7516. DOI: 10.1088/1475-7516/2021/06/046. URL: http://dx.doi.org/10.1088/1475-7516/2021/06/046.

[9] A. Abusleme et al. "TAO Conceptual Design Report: A Precision Measurement of the Reactor Antineutrino Spectrum with Sub-percent Energy Resolution". In: (2020). arXiv: 2005.08745 [physics.ins-det].

[10] R. Brun and F. Rademakers. "ROOT: An object oriented data analysis framework". In: *Nucl. Instrum. Meth. A* 389 (1997). Ed. by M. Werlen and D. Perret-Gallix, pp. 81–86. DOI: 10.1016/S0168-9002(97)00048-X.

[11] C. Ghabrous Larrea et al. "IPbus: a flexible Ethernet-based control system for xTCA hardware". In: *Journal of Instrumentation* 10.2 (2015). URL: https://cds.cern.ch/record/2020872/files/CR2014_334.pdf.

[12] CAEN SpA. https://www.caen.it/products/dt5810/. Accessed: 2021-08-31.

[13] Ethernet Alliance. *Ethernet Jumbo Frames*. http://www.ethernetalliance.org/wp-content/uploads/2011/10/EA-Ethernet-Jumbo-Frames-v0-1.pdf. Nov. 2009.